Materials and Design 119 (2017) 338–350

Contents lists available at ScienceDirect

Materials and Design

journal homepage: www.elsevier.com/locate/matdes

Additive manufacturing of cardiovascular CoCr stents by selective laser melting

Ali Gökhan Demir *, Barbara Previtali

Department of Mechanical Engineering, Politecnico di Milano, Via La Masa 1, 20156 Milan, Italy

HIGHLIGHTS

- SLM was used to produce CoCr prototype stents with PW laser emission.
- A prototype stent mesh employing design rules for SLM was proposed.
- Concentric scanning improved geometrical fidelity compared to hatching.
- Prototype stents were similar in surface roughness and microhardness compared to macro SLM components.
- The efficacy of electrochemical polishing depended on the correct selection of the SLM scan strategy.

GRAPHICAL ABSTRACT

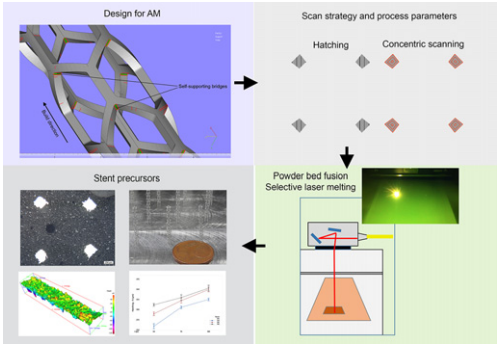

ARTICLE INFO

Article history:
Received 5 October 2016
Received in revised form 23 December 2016
Accepted 28 January 2017
Available online 1 February 2017

Keywords:
Selective laser melting
CoCr alloy
Stent
Biomedical device
Micro additive manufacturing
Micro computed tomography

ABSTRACT

In this work, the selective laser melting (SLM) of CoCr alloy powder for producing cardiovascular stents is investigated. The paper aims to assess the feasibility of producing a CoCr stent precursor through SLM as an alternative method to the conventional manufacturing cycle, which is based on microtube production and consecutive laser microcutting. Design rules for manufacturability are investigated, and a simple prototype design for additive manufacturing is proposed. The SLM process is investigated with an industrial system that utilises pulsed wave emission. Different scan strategies, namely hatching and concentric scanning, were used. Strut thickness and roughness, as well as chemical composition, were analysed. Representative conditions were further analysed by microhardness measurements and X-ray micro computed tomography. Electrochemical polishing was applied to assess the feasibility of surface finishing. The results show that SLM can be considered as a substitute operation to microtube manufacturing and laser microcutting for shaping precursors in stent manufacturing. Prototype stents with acceptable geometrical accuracy were achieved and surface quality could be improved through electrochemical polishing. The chemical composition remained unvaried, with a marginal increase in the oxide content.

1. Introduction

Cardiovascular stents are mesh-like structures used to restore normal blood flow following coronary artery obstruction [1]. The device has a diameter of between 1.2 and 2.5 mm, and is transported to the position in the artery where the intervention is required using a catheter.

* Corresponding author.
E-mail addresses: aligokhan.demir@polimi.it (A.G. Demir), barbara.previtali@polimi.it (B. Previtali).

http://dx.doi.org/10.1016/j.matdes.2017.01.091
0264-1275/

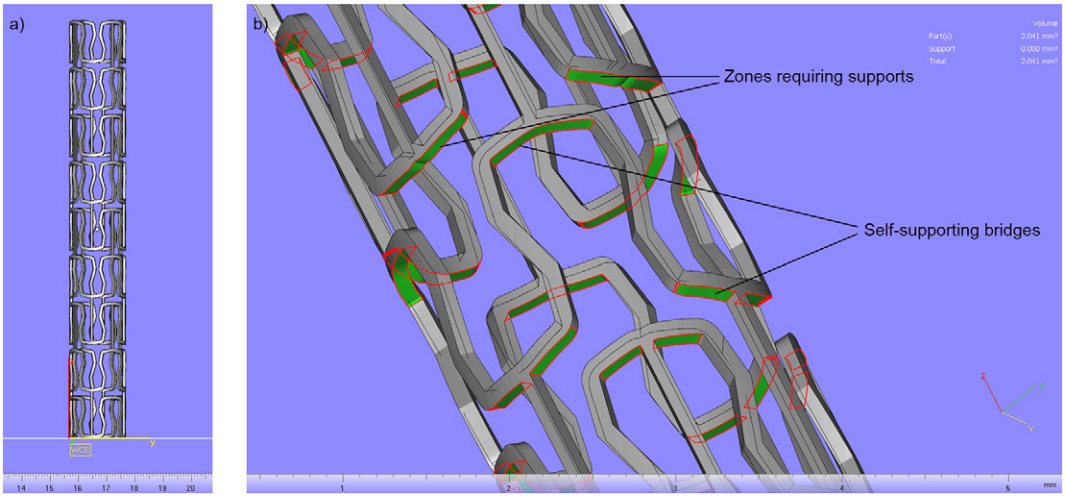

Fig. 1. a) Solid model of a stent resembling a commercial design (Magic Stent, Biotronik, Berlin, Germany). b) Highlighted zones correspond to surfaces with an angle of <45° with respect to the layer plane (xy). Some of these surfaces require supports due to no previous connection with the built structure.

After expansion, the final diameter ranges between 2 and 5 mm. The most widely deployed cardiovascular stents are made of stainless steel, titanium and CoCr alloys [2]. These stents are conventionally produced by way of a manufacturing chain, consisting in the use of tubular precursors, which are laser microcut into the stent mesh [3], followed by chemical and electrochemical surface cleaning stages [4,5]. Despite being an established production chain for most common stent materials, several improvements can be obtained, for example reduced production times and improved geometrical flexibility. Additive manufacturing processes based on powder bed fusion stand out as an appealing option for this purpose, which can be used to produce stent precursors directly from powder reducing minitube manufacturing and laser microcutting steps in a single process.

Selective laser melting (SLM) is a powder bed fusion technique, where a laser scans the powder layer by layer, generating the desired geometry. Some key advantages of SLM are shape flexibility and the use of lattice structures [6,7]. Adequately designed components employing these features have been found to reduce component weight, improve mechanical performance and even reduce production costs for large components. While the industrial and scientific communities are looking into improved productivity and the production of larger components, the use of SLM for obtaining micro components has received less attention. This is due to the limited process resolution, which can be expressed by layer thickness in build direction (20–50 μm) and smallest feature size on the scanning plane (400–500 μm) [8]. Even though these parameters can be regulated through more accurate displacement control and smaller beam sizes, the powder size stands as another limitation. The common powder size employed in the SLM process is between 20 and 50 μm, which allows for an effective melting, as well as good flowability [9]. Finer powders constitute further safety risks. Another issue regards the use of design for additive manufacturing rules in micrometric dimensions. While some of these rules are apparent for macro components, there is still a need for further studies in the micro field. Regenfuss et al. [10] used a novel SLM system for micro part manufacturing, which employed compression on the powder and an ns-pulsed fiber laser. In the produced components, the geometrical accuracy was very high, while internal porosity remained an issue [11–13].

The use of additive manufacturing techniques for vascular devices has been limited to a few applications using polymeric materials, together with processes such as fused deposition modelling [14], stereolithography [15] and binder jetting [16]. There is an apparent need for a comprehensive analysis of available and novel additive manufacturing techniques for metallic materials with adequate geometrical precision. Wessarges et al. used fine powder (5–20 μm) with a micro SLM system to produce prototype stents of AISI 316L stainless steel, which were subsequently finished by plasma and chemical polishing [17]. The prototype stents showed promising mechanical performance despite surface cracks after expansion. However, a more comprehensive analysis is required regarding the processing strategies

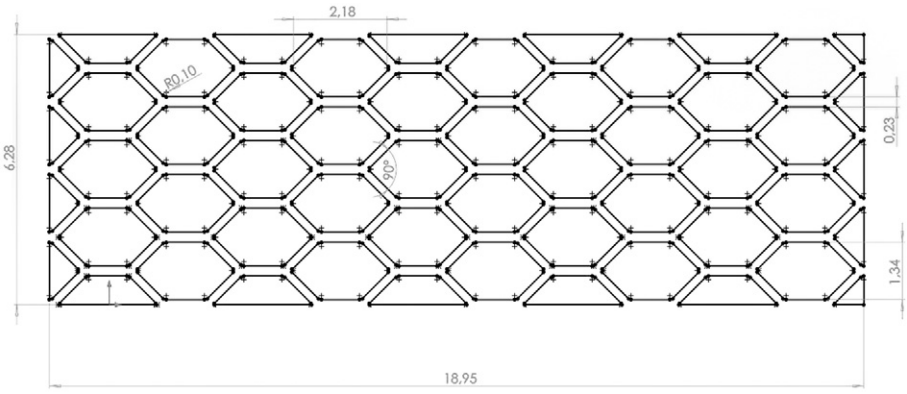

Fig. 2. Technical drawing of the designed stent prototype for selective laser melting.

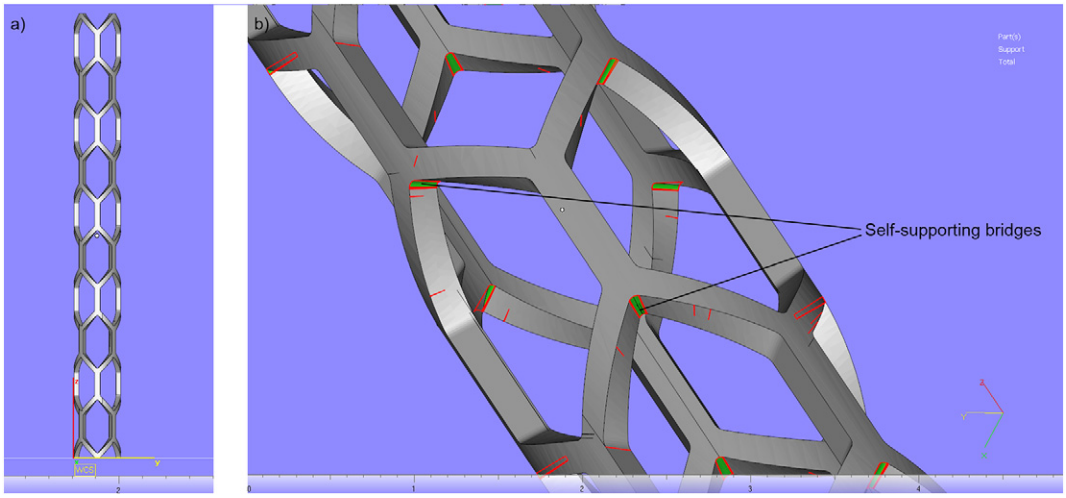

Fig. 3. a) Solid model of the designed stent prototype for selective laser melting. b) Highlighted zones correspond to surfaces with an angle of <45° with respect to the layer plane (xy).

available to industrial SLM systems in order to achieve the dimensional requirements without internal defects, as well as the design rules for additive manufacturing.

The lattice structures obtained in macro components are similar to stent form and dimensions. The use of long pulsed (μs-ms) fiber lasers presents further benefits for high precision in lattice and fine structures, due to the more controlled energy input into the material and better control of pulse disposition over the scan geometry [18–21].

Accordingly, this work investigates the use of an industrial SLM system for its feasibility in producing stent geometries. The assessment is carried out with an industrial SLM machine made mainly for medium-sized components, employing a pulsed wave, power modulated fiber laser, and industrial grade CoCr powder with shape and size developed for macro applications. At the initial stage, the design rules for the manufacturability of stent geometries through SLM is discussed. Different scan strategies for laser parameters are utilised in the experimental stage. Surface quality and strut dimensions are analysed to indicate further requirements for biomedical grade stent manufacturing. Preliminary analysis of surface finishing was carried out with electrochemical polishing. Process productivity is compared to the laser microcutting of a tubular precursor.

2. Design of the stent mesh for selective laser melting

Several rules should be considered when manufacturing components using SLM. These rules in particular regard part orientation, part thickness, overhang regions and support generation. Regions with an angle smaller than 45° with respect to the layer plane require supports. An overhang region is a zone suspended over non-molten powder and is connected to the rest of the component on a single side. Overhang regions can be built up to 1 mm without a support. Bridged gaps are also suspended over non-molten powder but are attached to the built component on both ends, which can be tolerated up to 4 mm. A minimum gap of 0.3 mm is recommended between separate features. The mentioned values are indicative and can vary between the different materials and systems used. These rules can, in most cases, be effectively implemented for existing large parts. However, the SLM process and the realized product perform at their best if manufacturing rules are considered at the design phase. These problems become more relevant on a micro product scale, as the feature dimensions come closer to the beam diameter, layer thickness and powder grain size.

A conventional stent mesh is designed in order to be suitable for being expanded in the artery, but also suitable for the manufacturing steps involving the laser microcutting of a microtube. Fig. 1 exhibits the 3D model of a stent resembling a commercial design (Magic Stent from Biotronik, Berlin) [22,23]. It can be seen that the best part orientation is vertical, as it limits the amount of support structures needed between the stent and the substrate plate. However, several zones exhibit the need for support structures due to being at an angle of <45°, as highlighted in green in Fig. 1.b. Most of these zones do not require the use of any support structures, because they are either overhang or bridge structures within the tolerable regions. These zones are highlighted as self-supporting bridges in Fig. 1.b. There are several other zones, which do not have any prior connection to the substrate plate. As the layers progress in the build direction (z-axis), all the zones except these have a direct connection with the previously molten layer. The zones requiring supports correspond to surfaces, which appear at a given layer without any connection to the previously molten layers and, during the process, the laser beam melts overhang powder. Heat accumulates in these regions, since the heat conduction of powder is less than that of the solid. Resultantly, the melting process becomes instable. Moreover, due to the missing mechanical connection with any previous layer, the molten zone is not anchored, therefore it is removed with the movement of the powder recoater Consequently, the stent build fails. Moreover, the removed parts move around the powder bed as debris, generating further irregularities on other parts.

In order to study the feasibility of the SLM process for stent manufacturing, a simple stent mesh was designed deriving from similar designs available commercially and reported in literature [3,24]. A final design was generated employing the specific design rules for additive manufacturing and without comprising the main functional requirement, namely expandability. The stent mesh reported in Fig. 2 was designed with a 200 μm strut thickness, 2 mm diameter and 18.95 mm length. The design implemented a simple zig-zag pattern, which

Table 1
Chemical composition of the CoCr powder declared by the producer.

Cr wt%	Mo wt%	Co wt%	O wt%	Si wt%	Mn wt%	Fe wt%	Ni wt%	N wt%	W wt%	Al wt%	Ti wt%
27–30	5–7	bal.	<0.10	<1.00	<1.00	<0.75	<0.50	<0.25	<0.20	<0.10	<0.1

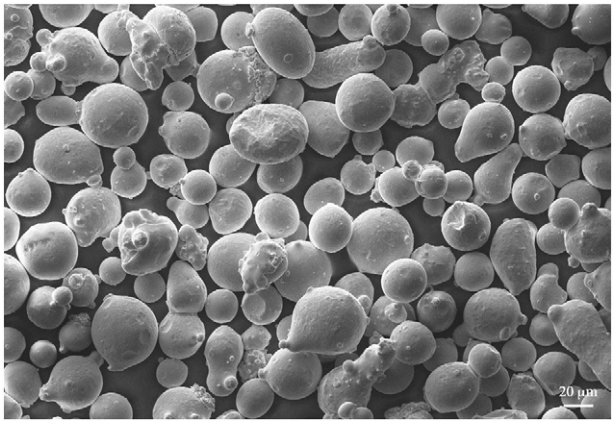

Fig. 4. Morphology of the CoCr powder used in the study.

avoided overhang zones and zones requiring support structures, suitable for a build orientation along its length. The design of this mesh can be categorised as closed cell with non-flex connectors [3]. The 2D design was projected over a 2 mm tube with 0.2 mm thickness to achieve the solid model. As the main concern of the study is to investigate the production method, no analysis or optimization was carried out on the mechanical performance of the design. Fig. 3.a reports the solid model of the new stent design. As seen in Fig. 3.b, the stent design does not exhibit any regions in need of support structures, and all regions with an orientation below 45° are self-supporting.

3. Materials and methods

3.1. CoCr powder

Throughout the study, CoCr powder with a chemical composition similar to the ASTM F75 alloy was used (LPW Technology, Cheshire, UK). The powder was gas atomized under Ar and spherical in shape. The average particle size was measured as 33 µm by laser diffraction. The apparent density of the powder was 5.04 g/cm^3, whereas the solid density was 8.3 g/cm^3. The nominal chemical composition is reported in Table 1, while the powder morphology can be seen in Fig. 4. For stent manufacturing, other CoCr alloys such as L606 are usually preferred [25–27]. CoCr alloys with a chemical composition similar to the present one are also used in bioimplant manufacturing [28,29]. In this study, this alloy was preferred as its processability by SLM has been demonstrated for larger components [20].

Table 2
Details of the experimental plan.

Strategy	Hatching	Concentric scanning
Fixed parameters		
Focal position, f (mm)	0	0
Point distance, d_p (µm)	90	40
Line distance, d_l (µm)	90	40
Layer thickness, z (µm)	30	30
Varied parameters		
Peak power, P_{peak} (W)	150; 165; 180	30; 40; 50
Pulse duration, t (µs)	50; 75; 100	100; 120; 140

3.2. Selective laser melting system

An industrial SLM system, Renishaw AM250, was used throughout the experimental work (Stone, UK). A 200 W active fiber laser was implemented in the system (R4 from SPI, Southampton, UK). The optical chain was composed of a galvanometric scanner with integrated z-axis positioner. The estimated beam diameter was 75 µm in the given combination. Prior to processing, a vacuum was applied to the processing chamber, taking it down to −950 mbar, and then it was filled with Ar, reaching an overpressure of 15 mbar. A circulation pump maintained the gas flow parallel to the powder bed. The oxygen content of the process chamber was maintained below 1000 ppm throughout the process.

The SLM system employed pulsed wave (PW) laser emission by power modulation, enabling control over different process parameters. In all of the scanning strategies, the laser was positioned on a certain point to emit a given peak power (P_{peak}) for a fixed pulse duration (t) in the µs range. These two parameters together determine the pulse energy ($E = P_{peak} \cdot t$). The laser jumped to the consecutive position on the scanned line, which was at a given point distance (d_p), and repeated the laser exposure. At the end of each scanned line, the laser jumped to the adjacent one, which was at a given line distance (d_l). Scan lines could be executed through the parallel hatching or concentric scanning of the layer geometry from the border to the core. The focal position (f) controlled the position of the beam focal point with respect to the powder bed surface. For the present system, negative focal position values refer to a laser spot focused above the powder bed surface, and positive values refer to a focal point below the powder bed surface. Layer thickness (z) was kept constant around the whole build. Magics 19 was used (Materialise, Leuven, Belgium) for slicing and post processing the layer trajectories. QuantAM build preparation software was employed (Renishaw, Stone, UK) for visualization of the scan trajectories.

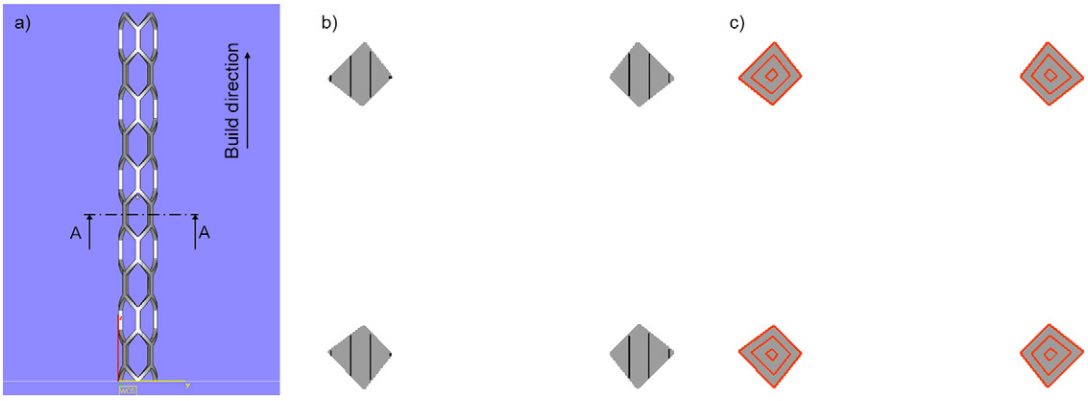

Fig. 5. Scan strategies used in the experimental study shown at an intermediate layer. a) Designed stent prototype and A-A section line depicting the layer in which the scan strategies are shown. b) Hatching strategy and c) concentric scanning strategies shown with black and red lines respectively, with the sectioned stent struts shown in grey.

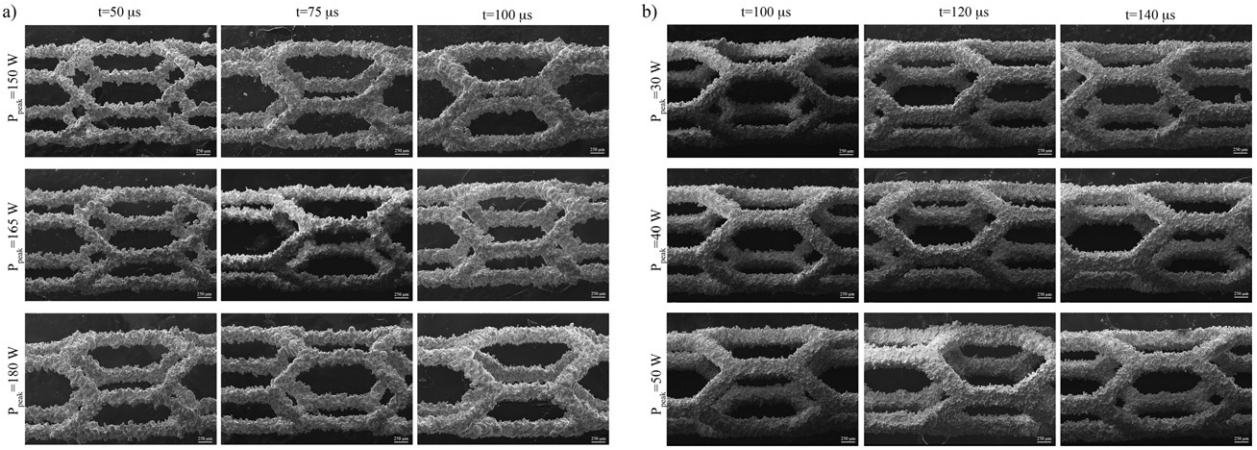

Fig. 6. SEM images of the CoCr prototype stents obtained with a) hatching and b) concentric scanning strategy. Build orientation is from left to right with respect to the orientation of the stents in the images.

3.3. Characterization equipment

Scanning electron microscopy images were taken and chemical composition was analysed using energy dispersive spectroscopy (EVO-50 from Carl Zeiss, Oberkochen, Germany). Strut thickness was measured using a universal horizontal measurement system (DMS 680 from Microrep Joint Instruments, Milan, Italy). Surface quality was characterized directly on the stent strut with focus variation microscopy (InfiniteFocus from Alicona Imaging GmbH, Graz, Austria). Images of the stent struts were taken with a 10× objective. The estimated vertical and lateral resolution values were 1.3 μm and 3.4 μm respectively. Surface roughness was measured over a 1.3 mm length on the struts. Cross-sections of the stent struts were taken perpendicular to the build direction at the layer plane (xy) and optical microscopy images were taken (Leitz Ergolux 200 from Leica, Wetzlar, Germany). Vickers microhardness was measured over the cross sections, with a 500 gf applied load and 15 s dwell time (VMHT 30A from Leica, Wetzlar, Germany). X-ray micro computed tomography was used to view internal defects (X25 MicroCT scanner from North Star Imaging, Rogers, MN, USA). A flat CMOS-type panel was employed. The source voltage and intensity were 160 kV and 20 μA respectively. The voxel size of the acquisitions was $3.9 \times 3.9 \times 3.9\ \mu m^3$.

3.4. SLM experimental plan

Two different scan strategies were tested to evaluate production feasibility. The first one consisted of parallel scan lines (see Fig. 5.b). This strategy is commonly used for scanning the main volume of larger parts, and at each layer the scan direction was varied by 67°. The second strategy consisted of closed and concentric trajectories, which followed the outer contour of the scanned geometry (see Fig. 5.c). This strategy is commonly used for finishing the borders of larger parts. Process

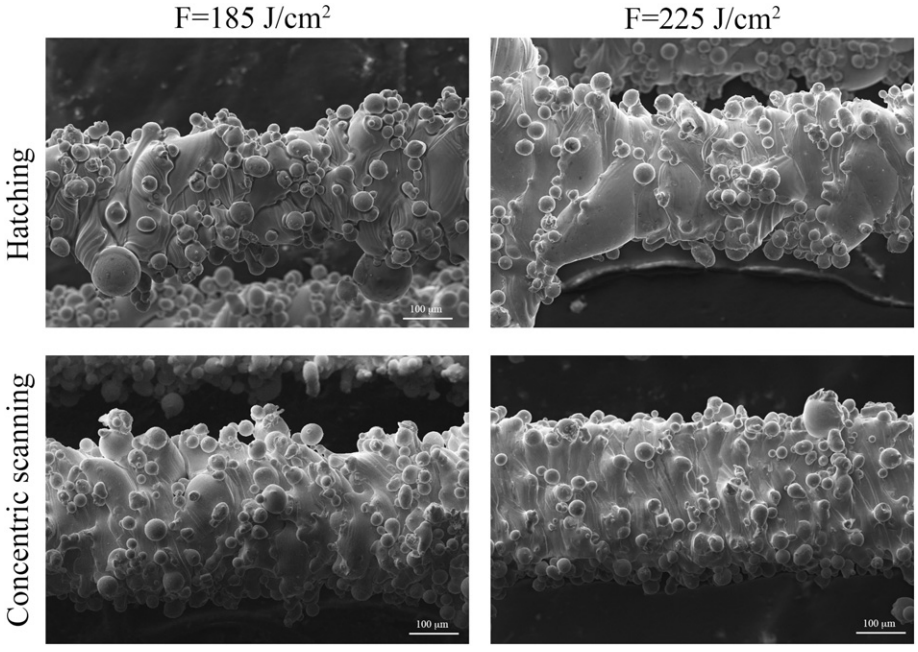

Fig. 7. Comparison of the CoCr prototype stent struts obtained with same fluence levels and different scan strategies. Hatching conditions: $P_{peak} = 150$ W; $t = 50$ μs; $F = 185$ J/cm^2; $P_{peak} = 180$ W; $t = 100$ μs; $F = 225$ J/cm^2. Concentric scanning conditions: $P_{peak} = 30$ W; $t = 100$ μs; $F = 185$ J/cm^2 $P_{peak} = 30$ W; $t = 120$ μs; $F = 225$ J/cm^2.

Table 3
ANOVA table for h (μm) obtained with hatching scan strategy.

Source	DF	Adj SS	Adj MS	F-value	*P*-value
P_{peak} (W)	2	11,390	5695.1	32.9	0
t (μs)	2	28,220	14,110.1	81.52	0
P_{peak} (W)* t (μs)	4	1562	390.5	2.26	0.078
Error	45	7789	173.1		
Total	53	48,961			

Table 4
ANOVA table for h (μm) obtained with concentric scan strategy.

Source	DF	Adj SS	Adj MS	F-value	*P*-value
P_{peak} (W)	2	1202	651.1	4.9	0.012
t (μs)	2	2224	1112	8.37	0.01
P_{peak} (W)* t (μs)	4	21.5	5.4	0.04	0.997
Error	45	5977	132.8		
Total	53	9525			

parameters were adapted starting from the conditions provided by the SLM system manufacturer for larger components. Point (d_p) and line (d_l) distances were kept equal, but different values were used for different scan strategies (90 μm and 40 μm for hatching and concentric scanning respectively). Focal position was fixed on the powder bed surface in all conditions ($f = 0$ mm), while a 30 μm layer thickness (z) was employed. Peak power and pulse duration were varied at 3 levels, according to a 3^2 factorial plan applied separately to each scan strategy. With the hatching strategy, higher peak powers ($P_{peak} = 150–180$ W) and moderate pulse durations ($t = 50–100$ μs) were preferred, corresponding to higher pulse energies ($E = 7.5–18$ mJ). With concentric scanning strategy, low peak powers ($P_{peak} = 30–50$ W) and higher pulse durations ($t = 100–140$ μs) were preferred, corresponding to lower pulse energies ($E = 3–9$ mJ). Fluence was used as a single parameter to compare the different scanning strategies calculated from the following equation:

$$F = \frac{P_{peak} \cdot t}{d_p \cdot d_l} \quad (1)$$

The corresponding fluence ranges were 93–222 J/cm^2 for hatching strategy and 187–438 J/cm^2 for concentric scanning strategy. Six replications were produced for each parameter combination. As response variables, strut thickness (h), average surface roughness (Ra), and chemical composition were evaluated. The dimensional error (e) in strut size was also calculated as:

$$e = h - h_n \quad (2)$$

where h_n is the nominal strut size. Analysis of variance (ANOVA) was applied with statistical significance level $\alpha = 5\%$. Details of the experimental plan are depicted in Table 2.

3.5. Electrochemical polishing

Cardiovascular stents produced by laser microcutting of microtubes are finished conventionally by electrochemical polishing. Feasibility of applying the same method for improving surface quality of the prototype stents was assessed. Electrochemical polishing was applied to representative prototype stents produced with the two scan strategies. The electrolyte was composed of 45 vol% sulfuric acid (H_2SO_4), 50 vol% phosphoric acid (H_3PO_4), and 5 vol% water [30]. A stainless steel (AISI 316L) cathode was used. Electrochemical polishing was applied at 25 °C with 10 V tension and 2.1 A/cm^2 current density for 3 min. Prototype stents were cleaned in water before and after electrochemical polishing and dried in air.

4. Results

4.1. Morphology of SLM produced stents

Fig. 6 reports the SEM images of the stents as a function of process parameters using hatching and concentric scan strategies. It can be observed that stent geometry is achievable with both of the scan strategies, although with a high surface roughness, being a characteristic of SLM produced parts also in macro scale [31,32]. The surface topography is composed of molten layer (around the strut width, >200 μm), sintered particles (20–50 μm) and smaller droplets of molten material (<20 μm). Concerning the conditions realized with the hatching strategy, the strut geometry is not well defined, and especially with low the pulse duration and peak power, the struts are irregular in thickness. Such irregularity is attributed to insufficient melting within the layers, which also generates irregular bonding between them. As a matter of fact, the separation lines between consecutive layers are visible. With increased pulse duration and peak power, strut thickness increases and becomes more regular. However, the morphology deviation persists, pointing out the inadequacy of the employed scan strategy for micro geometries. With concentric scanning, however, the stent geometry is much more defined. The struts are much more regular in thickness and the main surface irregularity is due to the molten material droplets. With increased pulse duration and peak power, strut regularity improves as the thickness increases.

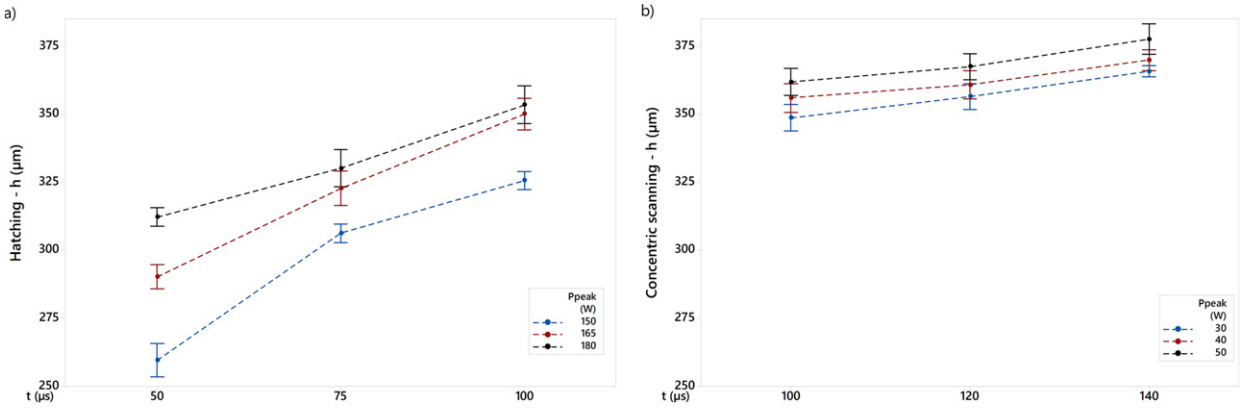

Fig. 8. Evolution of strut thickness as a function of process parameters and scanning strategy: a) hatching, b) concentric scanning. Error bars represent standard error.

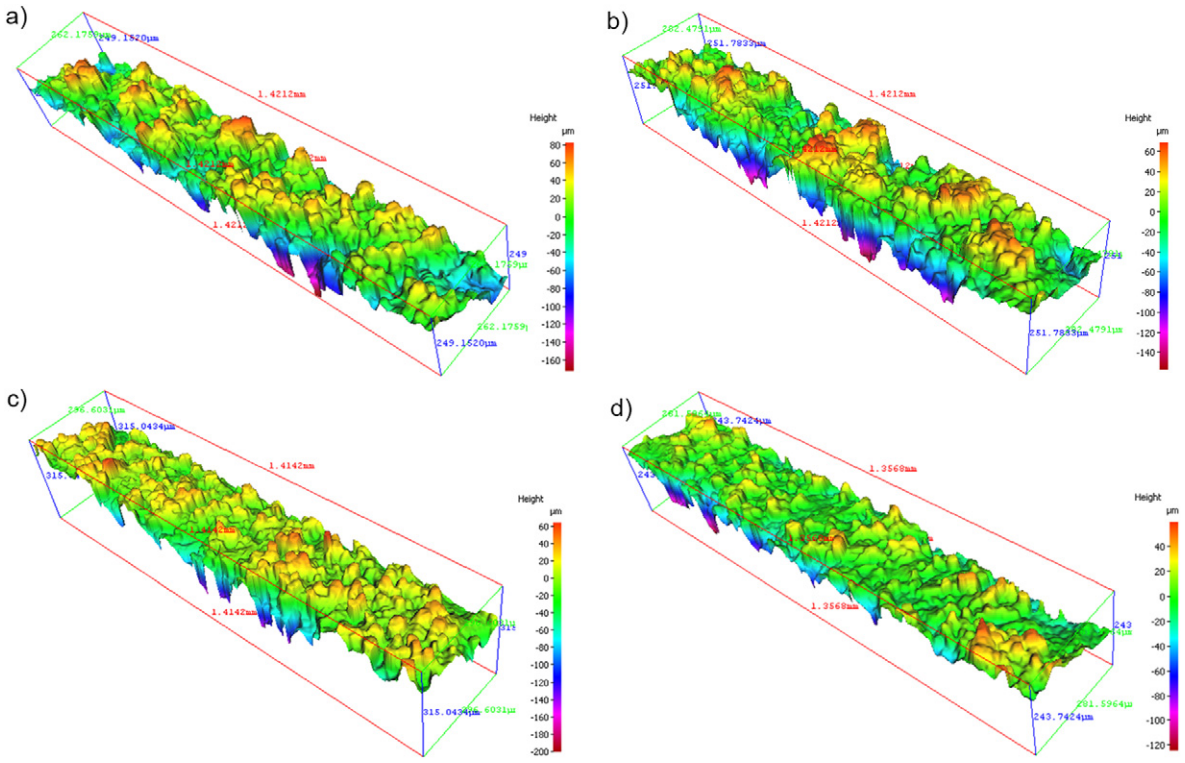

Fig. 9. Surface morphology of stent struts obtained with hatching (a, b) and concentric scanning (c, d). a) $P_{peak} = 150$ W, $t = 50$ µs; b) $P_{peak} = 180$ W, $t = 100$ µs; c) $P_{peak} = 30$ W, $t = 100$ µs; d) $P_{peak} = 50$ W, $t = 140$ µs.

In Fig. 7, different scan strategies are compared as a function of fluence. It can be seen that for both the scan strategies, the increase of fluence corresponds to strut enlargement. However, concentric scanning provides further improvement of bonding between different layers. Moreover, the designed rectangular section is achieved with concentric scanning, whereas the hatching strategy consistently produces an irregular section.

4.2. Strut thickness

Strut thickness measurements were coherent with the SEM image observations, depicting thicker struts (h = 340–380 µm) with concentric scanning than with the hatching strategy (h = 250–350 µm). The statistical significance of the process parameters was analysed for each scan strategy separately. The results of the ANOVA tests are summarized in Tables 3 and 4 respectively. In both cases, peak power and pulse duration were found to be significant and increased the strut thickness, whereas their interaction did not induce any significant change. Over the experimented region, pulse duration was found to have a higher influence for both of the scanning strategies as depicted by the F-values, as well as the plots exhibited in Fig. 8. The resultant error in strut size varies between 50 and 150 µm for hatching and 140–180 µm for concentric scanning.

4.3. Surface roughness

Fig. 9 reports the surface topography of the stent struts observed with focus variation microscopy. It can be seen that an increase in peak power and pulse duration appears to improve surface roughness. As observed in the SEM images, the surface quality is better with concentric scanning when compared to those obtained with the hatching strategy. Overall, the average surface roughness (*Ra*) measured over the stent strut varied between 10.5 and 13 µm for the ones obtained with hatching, and between 8.5 and 10 µm for those obtained with concentric scanning, which is comparable to the surface quality of macro parts [31,32]. Tables 5 and 6 report the ANOVA results for the response variable Ra with the use of hatching and concentric scanning respectively. With the hatching strategy, both peak power and pulse duration have significant effects on the surface roughness. As depicted in Fig. 10.a, the increase in both process parameters reduces the surface roughness. With the concentric scanning strategy, only peak power has a significant effect over the surface roughness in the experimented region (see Fig. 10.b). With concentric scanning, the significant parameter peak

Table 5
ANOVA table for Ra (µm) obtained with hatching scan strategy.

Source	DF	Adj SS	Adj MS	F-value	*P*-value
P_{peak} (W)	2	24.72	12.362	6.98	0.002
t (µs)	2	44.53	22.263	12.57	0
P_{peak} (W)* t (µs)	4	11.93	2.982	1.68	0.170
Error	45	79.72	1.772		
Total	53	160.90			

Table 6
ANOVA table for Ra (µm) obtained with concentric scan strategy.

Source	DF	Adj SS	Adj MS	F-value	*P*-value
P_{peak} (W)	2	19.248	9.6242	3.67	0.033
t (µs)	2	1.888	0.9438	0.36	0.699
P_{peak} (W)* t (µs)	4	9.509	2.3771	0.91	0.468
Error	45	117.880	2.6196		
Total	53	148.525			

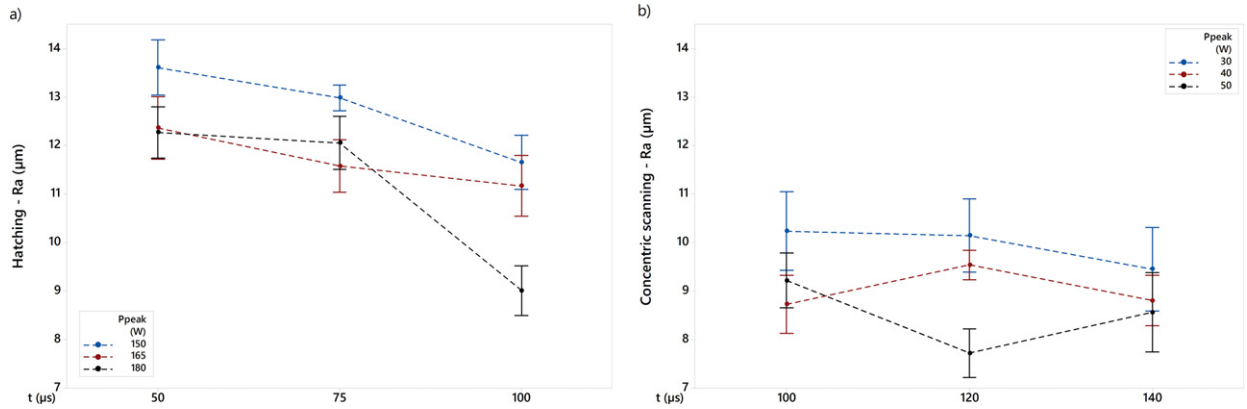

Fig. 10. Evolution of average surface roughness as a function of process parameters and scanning strategy: a) hatching, b) concentric scanning. Error bars represent standard error.

power induces, overall, around a 15% reduction in the average surface roughness, moving 30 W to 50 W.

4.4. Chemical composition

EDS analysis revealed that the chemical composition of the prototype stents consisted of the main alloying elements Co, Cr and Mo, with a limited amount of the secondary elements Mn, O and Si. Within a given strategy, no significant effect of processing parameters was found. The scan strategy did, however, induce very slight variations in the amount of the elements. Fig. 11 reports the chemical composition measurements along with the nominal composition limits for the revealed elements. It can be seen that the main alloying elements are within the nominal composition. In terms of secondary elements, the Mn and Si content appear to be within the expected region, whereas the O content is remarkably higher than the nominal value of the powder. The average value of oxygen found on the prototype stents was around 1% as opposed to the nominal 0.1 wt%.

4.5. Cross-section, microhardness, and CT scan

Cross-section, microhardness and CT scan analyses were carried out with representative conditions for each scanning strategy: for hatching $P_{peak} = 180$ W, $t = 100$ μs, for concentric scanning $P_{peak} = 40$ W, $t = 120$ μs. Fig. 12 exhibits the cross-section images of the whole prototype stents and one strut taken around the A-A section shown in Fig. 5.a. The cross-sections depict that full density is achieved with both scan strategies, and that the prototype stents are free of large pores. Nevertheless, loosely adhered particles and detached molten zones are visible around the struts, which generate deviations from the desired geometry (see Fig. 12.b). Microhardness measurements taken on the strut cross-section of the prototype stent were 321 ± 29 HV and 345 ± 32 HV for hatching and concentric scanning respectively. The microhardness values were found to be statistically same (result of ANOVA not reported for the sake of brevity).

Fig. 13 shows micro X-ray computed tomography images of the representative prototype stents obtained with the two scan strategies. The overall images (Fig. 13.a and c) are coherent with the SEM images, confirming that the stents are intact without breakage or discontinuities. The cross section images depict full density in white and voids in shades of black. The longitudinal cross-sections taken from the overall acquisitions (Fig. 13.b and d) show that the stents are free from large pores in the build direction. It can also be observed that geometrical integrity is better maintained with the concentric scanning strategy rather than with hatching. Transversal cross sections confirm the previous observations through physically cut specimens. The specimens are free of large defects also in the layer plane.

4.6. Preliminary assessment of surface finishing

Fig. 14 reports SEM images of the prototype stents after electrochemical polishing. The images underline the interaction between the initial surface conditions and the outcome of electrochemical polishing. It can be seen that the prototype stent obtained with hatching (Fig. 14.a and b) exhibits higher surface roughness compared to the one realized with concentric scanning (Fig. 14.c and d) also after electrochemical polishing. The average surface roughness of stent realized with hatching was 9.19 ± 0.30 μm, similar to the initial surface roughness. In the case of the prototype stent realized with concentric scanning, the large droplets and sintered particles are removed. The strut width is slightly

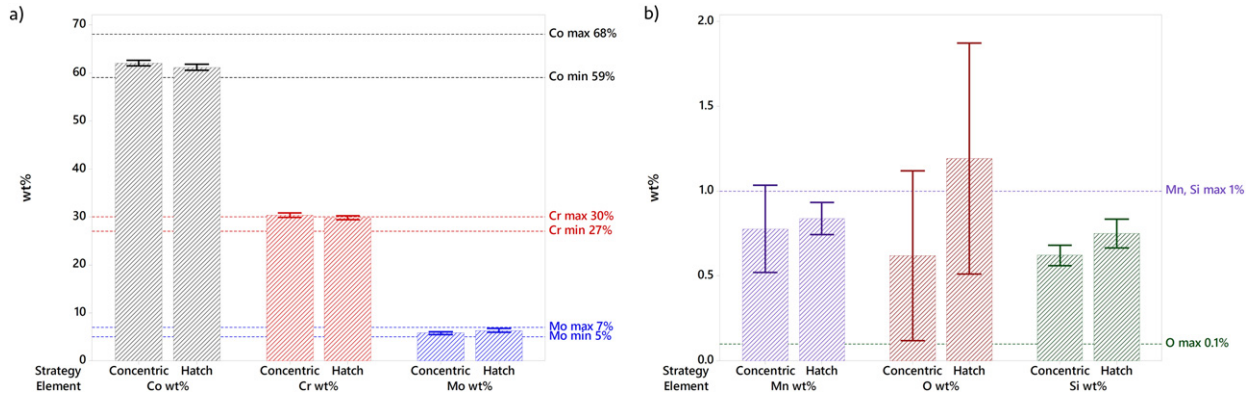

Fig. 11. Chemical composition of the prototype stents. a) Main alloying elements, b) secondary elements. Error bars represent 95% confidence interval for the mean.

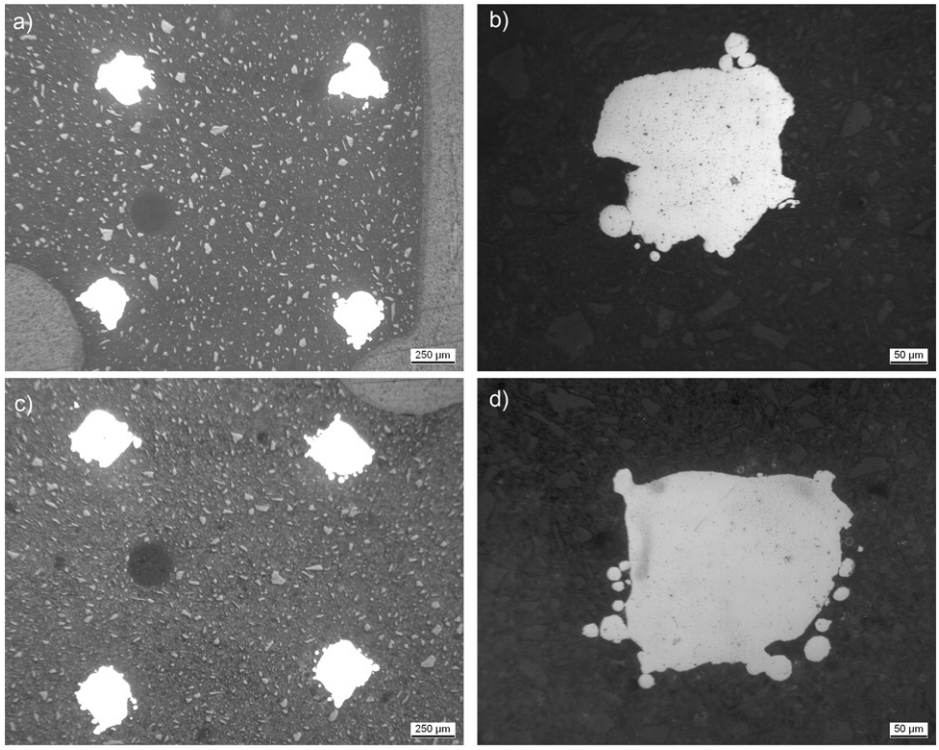

Fig. 12. Cross-section images of prototype stents obtained with a, b) hatching $P_{peak} = 180$ W, $t = 100$ µs and c, d) concentric scanning, $P_{peak} = 40$ W, $t = 120$ µs. a, c) Whole stents showing the four struts around the circumference; b, d) micrograph of a single strut.

reduced, the overall geometry is smoothed, and the underlying surface is free of cracks. The average surface roughness could be lowered to 1.45 ± 0.09 µm, corresponding to approximately 85% reduction. Despite the non-optimal surface finish, the results confirm the feasibility of employing the conventional finishing method on additively manufactured stents.

5. Discussion

The overall results depict that cardiovascular stents in CoCr can be produced in a near net-shape form through SLM, if certain design rules are respected. The main advantage of the SLM system used was the possibility of regulating the energy input by pulsed wave emission and the use of different scan strategies. The use of pulsed wave emission allows for accurate placement of laser pulses in short trajectories, as opposed to continuous linear scans employed with continuous wave emission. The produced prototype stents require further processing in order to improve the surface quality, as for biomedical applications the expected values of *Ra* are <0.5 µm. This fact implies that the chemical and electrochemical polishing stages should be further improved. Accordingly, geometrical integrity becomes of great importance at the SLM stage. As demonstrated by the results, concentric scanning improves the geometrical fidelity of the stents with micrometric dimensions. The use of higher peak power and pulse duration improves melting efficiency in both strategies. However, the same amount of fluence applied with different strategies shows that concentric scanning provides better geometrical definition. In all the investigated cases, the strut size, and resultantly the stent diameter, deviate from the nominal value due to the fact that no beam compensation was applied to the scan trajectories. It should be noted that the consecutive chemical and electrochemical etching steps necessary for obtaining the surface finish required by the stents will also remove a certain quantity of material. Beam compensation can be adjusted at the end of the processing cycle and iterations can be required to achieve the desired strut size.

The SLM process may induce loss of alloying elements depending on the processing conditions [33]. In the present work, the chemical composition of the produced stents was comparable to that of the used powder, whereas a slight increase in the oxide content was observed. The remaining oxygen content in the processing atmosphere is expected to be the reason for this increase. The surface oxide is critical for biocompatibility, but is expected to be removed during the consecutive cleaning stages [34]. In this study, an industrial grade CoCr alloy powder was employed for the main purpose of investigating the feasibility of the fabrication stages. The same alloy, but of higher purity, would be required for feasibility in biomedical applications.

The mechanical properties of the stents produced by SLM should match those produced conventionally. The gold standard of annealed AISI 316L stainless steel stents presents around 40% elongation, 170 MPa yield and 450 MPa ultimate tensile strength [35]. CoCr alloys produced through conventional manufacturing processes present higher yield (380–450 MPa) and ultimate tensile strengths (820–1200 MPa) with comparable elongation, which render them suitable for stent applications. In order to withstand the cyclic pulsations of the artery, the fatigue properties should also be adequate. It is preferable for a stent to have equiaxed grains of adequate size, allowing for the preservation of at least 5–10 grains along the strut thickness. Nonetheless, it is known that fast cooling cycles and the layer-by-layer build strategy generate columnar and small grains, deviating the material properties notably from their wrought and cast counterparts [36]. Moreover, the surface quality of stents produced using SLM can be problematic for fatigue properties, and internal defects such as pores should be minimal. As an indicator of their mechanical properties, the microhardness of the prototype stents is very similar to that of larger components reported in literature between 320 and 400 HV [20]. For comparison purposes, the

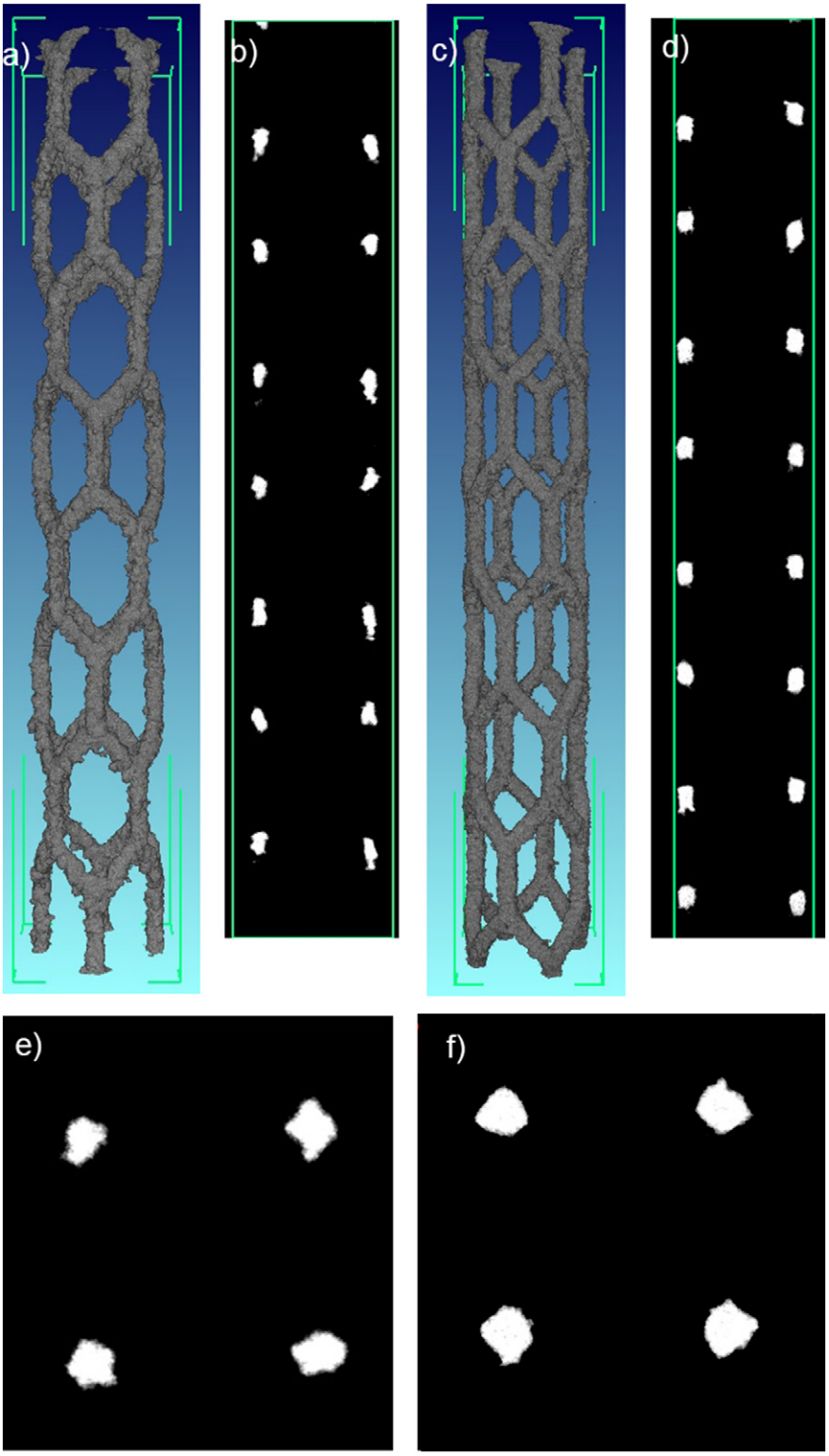

Fig. 13. Micro X-ray computed tomography images of the prototype stents obtained with a, b, e) hatching $P_{peak} = 180$ W, $t = 100$ μs and c, d, f) concentric scanning, $P_{peak} = 40$ W, $t = 120$ μs. a, c) Whole stents showing; b, d) longitudinal cross-sections; e, f) transversal cross-sections. Acquisition space is defined by the green outlines and corresponds to a) $2.47 \times 14.207 \times 2.47$ mm^3 and c) $2.271 \times 14.891 \times 2.536$ mm^3.

microhardness of wrought L605 CoCr alloy, which is more commonly employed for stent manufacturing, is between 220 and 300 HV [37]. The greater hardness of the SLM-produced CoCr alloy is attributed to the fast cooling cycles induced by laser irradiation. This implies that further heat treatment, in particular solution annealing, may be required to lower the hardness [38,39]. Heat treatment could also improve the mechanical behaviour of the stents by stress relieving, providing equiaxed grains and improving elongation [40]. The analyses showed that the stents are free of internal pores, but surface quality should be improved, also for fatigue resistance. The preliminary analysis on the surface finishing showed the possibility of using the conventional electropolishing method on additively

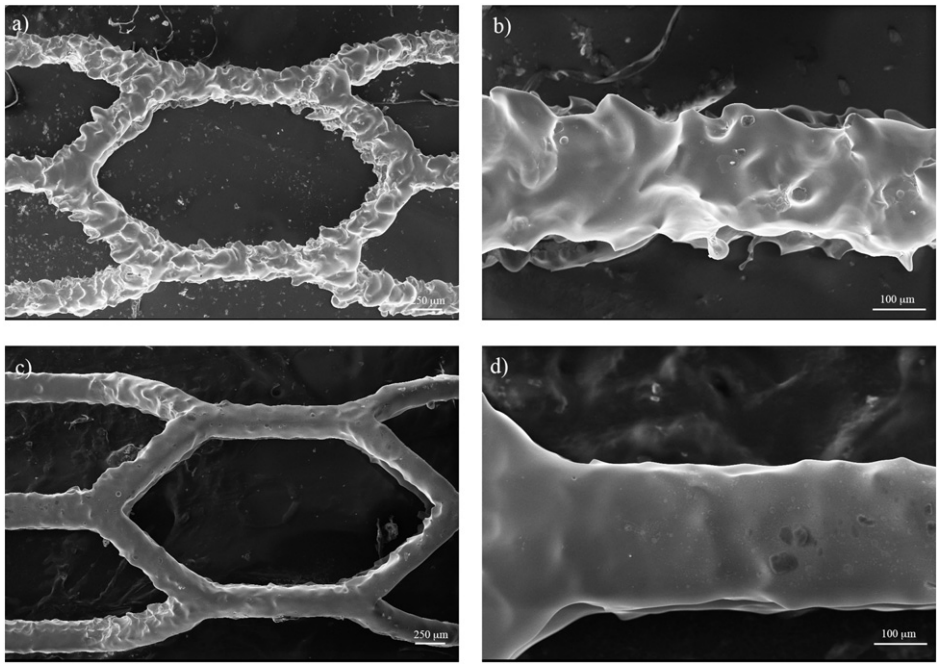

Fig. 14. SEM images of prototype stents after electrochemical polishing. Stent realized with a, b) hatching $P_{peak} = 180$ W, $t = 100$ µs and c, d) concentric scanning, $P_{peak} = 40$ W, $t = 120$ µs.

manufactured stents, although the conditions should be further optimized. Heat treatments and chemical/electrochemical finishing operations are part of the conventional manufacturing of cardiovascular stents based on laser microcutting of microtubes [41–43]. Hence, the necessity for heat treatment and finishing steps does not necessarily induce longer manufacturing cycles.

Another important factor regards productivity compared to the conventional manufacturing chain based on laser microcutting. The study shows that SLM can be allocated in the same production chain to reduce microtube manufacturing and laser micorcutting to a single-stage process. With a conservative spacing distance of 10 mm between the stents, it is possible to build 625 stents in a single batch in a 25×25 array on a build plate of 250×250 mm^2. With 8 s of powder recoating, the estimated material build rate for the highest peak power and longest pulse duration using the concentric scan strategy is 7.7 g/h. The estimated total build time is 3.3 h, which corresponds to 19 s for a single stent. In comparison, the duration of laser microcutting for producing the same stent mesh can be considered with a moderate cutting speed of 4 mm/s [44–46]. With a total cutting trajectory of 233 mm, the effective laser microcutting duration is 58 s, where the jump duration between consecutive cuts is neglected. The preliminary calculations depict that SLM can be highly productive as opposed to the conventional manufacturing route. However, it should be noted that the effective production time requires the addition of preparatory phases, which have not been considered here. Moreover, the surface quality produced by the SLM process conditions the duration and also the outcome of the consecutive cleaning steps. It has been previously demonstrated that rougher machining conditions require a longer chemical etching duration for laser microcut Mg alloy stents [47].

6. Conclusions

In this work, the use of SLM for producing cardiovascular stents using a CoCr alloy was assessed. The main aim of the paper was to demonstrate the feasibility of producing stent precursors through SLM as an alternative method to the conventional manufacturing cycle based on microtube manufacturing and laser microcutting. An industrial SLM system with a PW single mode fiber laser was used for the study. The design rules for producing a stent mesh without the use of support structures is discussed. Prototype stents were produced employing different scan strategies. The main outcomes of the work can be summarized as follows.

- Geometrical fidelity depends highly on the scan strategy, where concentric scanning is found to be suitable for generating the fine mesh.
- Increased laser peak power and pulse duration enlarge the strut and reduce the surface roughness.
- Control over the stent dimensions should be achieved through beam compensation rather than by changing the process parameters. The scan trajectory should be compensated after the allowance required for the post-processing steps has been assessed correctly.
- Conventional electrochemical polishing is suited for finishing additively manufactured stents. There is a strong interaction between the SLM parameters and electropolishing outcome. Surface quality can be improved removing loosely adhered particles and molten material to reveal the underlying geometry.
- The position of SLM in cardiovascular stent manufacturing can be allocated as a single step process, which substitutes microtube production based on extrusion and tube drawing, and the consecutive laser microcutting. At the current technological level, net-shape manufacturing is not possible because of the surface quality and mechanical properties that are required.
- SLM productivity can outperform the conventional stent manufacturing scheme. The additive manufacturing process merges microtube manufacturing and laser microcutting phases into a single step method. Moreover, several stents can be produced at a single build, further reducing the production cycle time. For a comprehensive analysis over productivity, the consecutive heat treatment and surface finishing operations should be further investigated.

Despite several advantages, the use of additive manufacturing for producing cardiovascular stents requires further attention on several points. The chemical and electrochemical finishing operations of the SLM-produced stents should be optimized. Mechanical performance in terms of tensile strength, recoil and fatigue resistance should be studied.

Despite the common use of a CoCr alloy for cardiovascular stents, the biocompatibility of SLM should be assessed due to the specific production conditions involved.

Acknowledgements

The authors gratefully acknowledge the support of Paolo Colombo during the design and experimental phases. Dr. Carlo Biffi is acknowledged for his support during the electrochemical polishing phase. This work was supported by Regione Lombardia under the call “Creatività: Eventi e Luoghi per L'innovazione nella Moda e nel Design, Linea 2: Infrastrutturazione Fisica e Digitale”.

Appendix A. The productivity estimation for the SLM process was carried out with a Matlab code developed in-house. The following parameters were considered in the calculations

Table A.1
Powder dosing and scanning related parameters used in the SLM productivity calculations.

Parameter	Value
Powder dosing and recoating time	8 s
Vector start delay	0 μs
Vector end delay	400 μs
Jump speed	5 m/s
Jump delay	500 μs
Total height	19 mm
Stent volume	4.89 mm^3

References

[1] P. Serruys, P. De Jaeger, F. Kiemeneij, C. Macaya, W. Rutsch, G. Heyndrickx, H. Emanuelsson, J. Marco, V. Legrand, P. Materne, J. Belardi, U. Sigwart, A. Colombo, J. Goy, P. Van den Heuvel, J. Delcan, M. Morel, A comparison of balloon-expandable-stent implantation with balloon angioplasty in patients with coronary artery disease, N. Engl. J. Med. 331 (8) (1994) 489–495.
[2] B.P. Murphy, P. Savage, P.E. McHugh, D.F. Quinn, The stress–strain behavior of coronary stent struts is size dependent, Ann. Biomed. Eng. 31 (6) (Jun. 2003) 686–691.
[3] D. Stoeckel, C. Bonsignore, S. Duda, M. Dunitz, A survey of stent designs, Minim. Invasive Ther. Allied Technol. 11 (4) (Jul. 2002) 137–147.
[4] H. Zhao, R. Stalmans, J. van Humbeeck, I. de Scheerder, Pickling of laser-cut NiTi slotted tube stents: effect on surface morphology, dimension changes and mechanical behaviour, J. Phys. IV 112 (Oct. 2003) 1125–1128.
[5] H. Zhao, J. Van Humbeeck, J. Sohier, I. De Scheerder, Electrochemical polishing of 316L stainless steel slotted tube coronary stents, J. Mater. Sci. Mater. Med. 13 (10) (Oct. 2002) 911–916.
[6] C. Yan, L. Hao, A. Hussein, D. Raymont, Evaluations of cellular lattice structures manufactured using selective laser melting, Int. J. Mach. Tools Manuf. 62 (2012) 32–38.
[7] C. Yan, L. Hao, A. Hussein, P. Young, D. Raymont, Advanced lightweight 316L stainless steel cellular lattice structures fabricated via selective laser melting, Mater. Des. 55 (2014) 533–541.
[8] R. Stamp, P. Fox, W. O'Neill, E. Jones, C. Sutcliffe, The development of a scanning strategy for the manufacture of porous biomaterials by selective laser melting, J. Mater. Sci. Mater. Med. 20 (9) (2009) 1839–1848.
[9] A.B. Spierings, N. Herres, G. Levy, C. Buchs, Influence of the particle size distribution on surface quality and mechanical properties in additive manufactured stainless steel parts, Solid Free. Fabr. Symp. (2010) 397–406.
[10] P. Regenfuss, A. Streek, L. Hartwig, S. Klötzer, T. Brabant, M. Horn, R. Ebert, H. Exner, Principles of laser micro sintering, Rapid Prototyp. J. 13 (4) (2007) 204–212.
[11] A. Streek, P. Regenfuss, R. Ebert, Laser micro sintering–a quality leap through improvement of powder packing, Proc. 19th Annu. SFF Symp. (2008) 297–308.
[12] H. Exner, M. Horn, A. Streek, F. Ullmann, L. Hartwig, P. Regenfuß, R. Ebert, Laser micro sintering: a new method to generate metal and ceramic parts of high resolution with sub-micrometer powder, Virtual Phys. Prototyp. 3 (2008) 3–11 (no. April 2014).
[13] P. Regenfuss, L. Hartwig, S. Klötzer, R. Ebert, T. Brabant, T. Petsch, H. Exner, Industrial freeform generation of microtools by laser micro sintering, Rapid Prototyp. J. 11 (1) (2005) 18–25.
[14] C. Spadaccio, F. Nappi, F. De Marco, P. Sedati, F.W.H. Sutherland, M. Chello, M. Trombetta, A. Rainer, Preliminary in vivo evaluation of a hybrid armored vascular graft combining electrospinning and additive manufacturing techniques, Drug Target Insights 10 (2016) 1–7.
[15] A.D. Lantada, A. de Blas Romero, E.C. Tanarro, Micro-vascular shape-memory polymer actuators with complex geometries obtained by laser stereolithography, Smart Mater. Struct. 25 (6) (2016) 65018.
[16] S.S. Moore, K.J. O'Sullivan, F. Verdecchia, Shrinking the supply chain for implantable coronary stent devices, Ann. Biomed. Eng. 44 (2) (2016) 497–507.
[17] Y. Wessarges, R. Hagemann, M. Gieseke, C. Nölke, S. Kaierle, W. Schmidt, K.P. Schmitz, H. Haferkamp, Additive manufacturing of vascular implants by selective laser melting, Biomed. Tech. 59 (2014) S401–S404.
[18] Z.S. Bagheri, D. Melancon, L. Liu, R.B. Johnston, D. Pasini, Compensation strategy to reduce geometry and mechanics mismatches in porous biomaterials built with Selective Laser Melting, J. Mech. Behav. Biomed. Mater. (2016) 1–11.
[19] B. Brown, W. Everhart, J. Dinardo, Characterization of bulk to thin wall mechanical response transition in powder bed AM, 26th Annu. Int. Solid Free. Fabr. Symp. (2015) 501–513.
[20] X. Zhou, D. Wang, X. Liu, D. Zhang, S. Qu, J. Ma, G. London, Z. Shen, W. Liu, 3D-imaging of selective laser melting defects in a Co-Cr-Mo alloy by synchrotron radiation micro-CT, Acta Mater. 98 (2015) 1–16.
[21] X. Zhou, K. Li, D. Zhang, X. Liu, J. Ma, W. Liu, Z. Shen, Textures formed in a CoCrMo alloy by selective laser melting, J. Alloys Compd. 631 (2015) 153–164.
[22] R. Waksman, R. Pakala, P.K. Kuchulakanti, R. Baffour, D. Hellinga, R. Seabron, F.O. Tio, E. Wittchow, S. Hartwig, C. Harder, R. Rohde, B. Heublein, A. Andreae, K.-H. Waldmann, A. Haverich, Safety and efficacy of bioabsorbable magnesium alloy stents in porcine coronary arteries, Catheter. Cardiovasc. Interv. 68 (4) (Oct. 2006) 607–617.
[23] W. Wu, L. Petrini, D. Gastaldi, T. Villa, M. Vedani, E. Lesma, B. Previtali, F. Migliavacca, Finite element shape optimization for biodegradable magnesium alloy stents, Ann. Biomed. Eng. 38 (9) (Sep. 2010) 2829–2840.
[24] A. Schuessler, U. Bayer, G. Siekmeyer, R. Steegmueller, M. Strobel, A. Schuessler, Manufacturing of stents: optimize the stent with new manufacturing technologies, New Technol. Vasc. Biomater. (2007) 93–106.
[25] P. Poncin, J. Proft, Stent tubing: understanding the desired attributes, Proc. ASM Conf. Mater. Process. Med. Devices (September) (2003) 253–259.
[26] H.M. Nef, H. Möllmann, M. Weber, W. Auch-Schwelk, T. Bonzel, J. Varelas, T.K. Nordt, J. Schofer, H.H. Minden, J. Stumpf, S. Schneider, A. Elsässer, C.W. Hamm, Cobalt-chrome MULTI-LINK VISION™-stent implantation in diabetics and complex lesions: results from the DaVinci-Registry, Clin. Res. Cardiol. 98 (11) (2009) 731–737.
[27] G. Khatibi, M. Lederer, A. Betzwar Kotas, M. Frotscher, A. Krause, S. Poehlmann, High-cycle fatigue behavior of thin-walled CoCr tubes, Int. J. Fatigue 80 (2015) 103–112.
[28] L. Reclaru, P.Y. Eschler, R. Lerf, A. Blatter, Electrochemical corrosion and metal ion release from Co-Cr-Mo prosthesis with titanium plasma spray coating, Biomaterials 26 (23) (2005) 4747–4756.
[29] C. Song, Y. Yang, Y. Wang, D. Wang, J. Yu, Research on rapid manufacturing of CoCrMo alloy femoral component based on selective laser melting, Int. J. Adv. Manuf. Technol. 75 (1–4) (2014) 445–453.
[30] C. Kaufmann, G. Mani, D. Marton, D. Johnson, C.M. Agrawal, Long-term stability of self-assembled monolayers on electropolished L605 cobalt chromium alloy for stent applications, J. Biomed. Mater. Res. - Part B Appl. Biomater. 98 B (2) (2011) 280–289.
[31] N.T. Aboulkhair, I. Maskery, C. Tuck, I. Ashcroft, N.M. Everitt, The microstructure and mechanical properties of selectively laser melted AlSi10Mg: the effect of a conventional T6-like heat treatment, Mater. Sci. Eng. A 104 (2016) 174–182.
[32] M. Król, L. Dobrzański, I. Reimann, Surface quality in selective laser melting of metal powders, Arch. Mater. Sci. 60 (2) (2013) 87–92.
[33] X. Zhao, B. Song, Y. Zhang, X. Zhu, Q. Wei, Y. Shi, Decarburization of stainless steel during selective laser melting and its influence on Young's modulus, hardness and tensile strength, Mater. Sci. Eng. A 647 (2015) 58–61.
[34] V. Milleret, A. Ziogas, S. Buzzi, R. Heuberger, A. Zucker, M. Ehrbar, Effect of oxide layer modification of CoCr stent alloys on blood activation and endothelial behavior, J. Biomed. Mater. Res. B Appl. Biomater. 103 (3) (2015) 629–640.
[35] S.D. Washko, G. Aggen, Wrought stainless steels, ASM Handbook, Vol. 1, ASM International 1990, pp. 841–907.
[36] B. Song, X. Zhao, S. Li, C. Han, Q. Wei, S. Wen, J. Liu, Y. Shi, Differences in microstructure and properties between selective laser melting and traditional manufacturing for fabrication of metal parts: a review, Front. Mech. Eng. 10 (2) (2015) 111–125.
[37] ASTM International, ASTM Standard F90-09, Specification for Wrought Cobalt–20Chromium–15Tungsten–10Nickel Alloy for Surgical Implant Applications (UNS R30605), 2009.
[38] J. Cawley, J.E.P. Metcalf, A.H. Jones, T.J. Band, D.S. Skupien, A tribological study of cobalt chromium molybdenum alloys used in metal-on-metal resurfacing hip arthroplasty, Wear 255 (7–12) (2003) 999–1006.
[39] C.V. Vidal, A.I. Muñoz, Effect of thermal treatment and applied potential on the electrochemical behaviour of CoCrMo biomedical alloy, Electrochim. Acta 54 (6) (2009) 1798–1809.
[40] B. Song, S. Dong, Q. Liu, H. Liao, C. Coddet, Vacuum heat treatment of iron parts produced by selective laser melting: microstructure, residual stress and tensile behavior, Mater. Des. 54 (2014) 727–733.
[41] A. Raval, A. Choubey, C. Engineer, D. Kothwala, Development and assessment of 316LVM cardiovascular stents, Mater. Sci. Eng. A 386 (1–2) (Nov. 2004) 331–343.
[42] Y.P. Kathuria, Laser microprocessing of metallic stent for medical therapy, J. Mater. Process. Technol. 170 (3) (Dec. 2005) 545–550.
[43] A.G. Demir, B. Previtali, Q. Ge, M. Vedani, W. Wu, F. Migliavacca, L. Petrini, C.A. Biffi, M. Bestetti, Biodegradable magnesium coronary stents: material, design and fabrication, Int. J. Comput. Integr. Manuf. 27 (10) (2014) 936–945.

[44] A.G. Demir, B. Previtali, C.A. Biffi, Fibre laser cutting and chemical etching of AZ31 for manufacturing biodegradable stents, Adv. Mater. Sci. Eng. 2013 (2013) 1–11.
[45] N. Muhammad, D. Whitehead, A. Boor, L. Li, Comparison of dry and wet fibre laser profile cutting of thin 316L stainless steel tubes for medical device applications, J. Mater. Process. Technol. 210 (15) (Nov. 2010) 2261–2267.
[46] N. Muhammad, D. Whitehead, A. Boor, W. Oppenlander, Z. Liu, L. Li, Picosecond laser micromachining of nitinol and platinum–iridium alloy for coronary stent applications, Appl. Phys. A Mater. Sci. Process. 106 (3) (Oct. 2011) 607–617.
[47] A.G. Demir, B. Previtali, Comparative study of CW, nanosecond- and femtosecond-pulsed laser microcutting of AZ31 magnesium alloy stents, Biointerphases 9 (2) (2014) 29004.